

The massive star binary fraction in young open clusters - II. NGC 6611 (Eagle Nebula)

H. Sana^{1,2*}, E. Gosset^{3†} and C. J. Evans⁴

¹European Southern Observatory, Alonso de Cordova 1307, Casilla 19001, Santiago 19, Chile

²Sterrenkundig Instituut Anton Pannekoek, Universiteit van Amsterdam, Postbus 94249, 1098 XH Amsterdam, The Netherlands

³Astrophysical Institute, Liège University, Bât. B5c, Allée du 6 Août 17, B-4000 Liège, Belgium

⁴UK Astronomy Technology Centre, Royal Observatory Edinburgh, Blackford Hill, Edinburgh EH9 3HJ, UK

Accepted 1988 December 15. Received 1988 December 14; in original form 1988 October 11

ABSTRACT

Based on a set of over 100 medium- to high-resolution optical spectra collected from 2003 to 2009, we investigate the properties of the O-type star population in NGC 6611 in the core of the Eagle Nebula (M16). Using a much more extended data set than previously available, we revise the spectral classification and multiplicity status of the nine O-type stars in our sample. We confirm two suspected binaries and derive the first SB2 orbital solutions for two systems. We further report that two other objects are displaying a composite spectrum, suggesting possible long-period binaries. Our analysis is supported by a set of Monte-Carlo simulations, allowing us to estimate the detection biases of our campaign and showing that the latter do not affect our conclusions. The absolute minimal binary fraction in our sample is $f_{\min} = 0.44$ but could be as high as 0.67 if all the binary candidates are confirmed. As in NGC 6231 (see Paper I), up to 75% of the O star population in NGC 6611 are found in an O+OB system, thus implicitly excluding random pairing from a classical IMF as a process to describe the companion association in massive binaries. No statistical difference could be further identified in the binary fraction, mass-ratio and period distributions between NGC 6231 and NGC 6611, despite the difference in age and environment of the two clusters.

Key words: binaries: close – binaries: spectroscopic – stars: early-type – open clusters and associations: individual: NGC 6611

1 INTRODUCTION

At a distance of ~ 2 kpc, NGC 6611 at the core of the Eagle Nebula (M16) is one of the most famous star-formation regions of the Southern sky. Popularised by the dramatic HST image of Hester et al. (1996), the striking morphology of the nebula is the result of the feedback of the massive stars in its core on the original natal cloud. In the last 6 Myr, M16 seems to have developed a continuous star-formation history, resulting in a diverse stellar population that encompasses high- and intermediate-mass stars, low-mass pre-main sequence stars, young embedded objects, maser sources and Herbig-Haro objects. As such, the Eagle Nebula is also one of the best places to study the positive and negative influence of young massive stars to trigger new formation events. Oliveira (2008) has recently reviewed star formation in the Eagle Nebula, so that we only provide here some of the key facts that are of direct interest for the present work.

Table 1. Brief comparison of the properties of the various spectrographs used to assemble our data set. The last column provides the number of epochs n obtained with each spectrograph.

Spectrograph	$\lambda\lambda$ range (\AA)	Resolving power	n
FEROS	3800-9200	48 000	78
FLAMES-GIRAFFE ^a	3850-4755, 6380-6620	20 850-29 600	10
FLAMES-UVES	4140-6210	47 000	6
UVES	3280-4560	80 000	3
ISIS	3800-5100, 6200-6800	7000	1

a. Each of the GIRAFFE epochs is actually composed of several observations using different wavelength settings. See Evans et al. (2005) for more information.

Several authors have identified variable extinction across the cluster and an abnormal reddening law. These properties have strongly affected the distance determination and a wide range of values, from 1.7 to 3.2 kpc, can be found in the literature. Yet, all the recent works seem to converge towards the closest distances. In the following, we

* E-mail: hsana@eso.org

† FNRS, Belgium

Table 2. Number of radial velocity (RV) measurements obtained for each object with respect to the considered spectral lines. ‘–’ means that the corresponding line has not been measured.

Object	He I λ4026	Si IV λ4089	He I λ4144	He I λ4388	He I λ4471	Mg II λ4481	He II λ4542	He II λ4686	He I λ4922	He II λ5412	He I λ5876	He I λ7065
BD-13°4923	11	11	10	12	12	10	12	13	9	10	10	9
BD-13°4927	7	7	–	8	8	8	8	8	6	8	6	6
BD-13°4928	7	7	7	8	8	–	8	8	6	6	6	6
BD-13°4929	11	11	11	11	12	–	12	12	–	10	10	–
BD-13°4930	7	7	7	8	8	8	8	8	6	6	6	5
HD 168075	9	9	9	9	11	11	11	11	11	11	9	8
HD 168076	9	–	–	–	7	–	7	7	–	7	7	–
HD 168137	14	14	14	14	14	14	14	14	13	14	14	12
HD 168183	13	13	13	13	13	–	13	13	13	13	13	13

adopt $d = 1.8 \pm 0.1$ kpc as found by Dufton et al. (2006) from the spectroscopic parallaxes of 24 OB stars.

The cluster age is 2-3 Myr typically, although the age spread is probably significant and extends from 1 to 6 Myr. The most recent age determinations (Bonatto et al. 2006; Martayan et al. 2008) seem to favour an even younger age around 1.5 Myr. Regarding the cluster mass, Bonatto et al. (2006) argued that the OB-type stars alone amount for a minimal mass of $\sim 1.6 \times 10^3 M_{\odot}$, although Wolff et al. (2007) suggested that the total mass could be as large as $\sim 2.5 \times 10^4 M_{\odot}$.

As the second paper in our series, this work mainly focuses on the multiplicity properties of the O-type star population in NGC 6611. Yet, given that those objects are the main source of radiative and kinetic energy of the Eagle Nebula, the present study has implications beyond the sole properties of the O-type stars in the cluster. It forms a prerequisite to any detailed understanding of the energetic balance of the mechanisms at work in the nebula.

With 13 O-type stars and about 50 B0 to B5 stars, the young open cluster NGC 6611 at the core of the Eagle Nebula hosts a rich early-type population. Compared to NGC 6231 (Sana et al. 2008, Paper I), the O star population in NGC 6611 is definitely younger and contains earlier spectral types. While several authors have investigated the multiplicity of these objects, the picture is still not complete. Bosch et al. (1999) obtained multi-epoch low- ($R \approx 4000$) and medium- to high-resolution ($R \approx 9000 - 15000$) spectroscopy of ten of the brightest OB stars and reported three definite binaries and three multiple candidates. Subsequent medium- to high-resolution ($R \approx 7000 - 29000$) spectroscopy by Evans et al. (2005) and Martayan et al. (2008) confirmed two of the known O-type binaries, further suggesting an additional SB1 candidate not observed by Bosch et al. (1999). All in all, the minimum binary fraction f_{\min} is $3/13 \approx 0.23$. It could however be much higher given that some objects lack multi-epoch monitoring and that four other binary candidates have been identified.

On the very large separation side, the adaptive optics survey of Duchêne et al. (2001) shed a complementary light on the multiplicity properties of the cluster. Focusing in the separation range from 200 to 3000 A.U. ($\approx 0.1-1.5''$) around 60 OB-type cluster members, they identified low-mass visual companions in $18 \pm 6\%$ of the cases, two of which are around O-type stars.

Finally, Gvaramadze & Bomans (2008) have recently

identified three O-type stars that have most likely been ejected from NGC 6611. Given the number of known O stars in the cluster (either isolated or within a multiple object), those ejected stars would amount to about 20% of the initial O-type star population in NGC 6611. Gvaramadze & Bomans (2008) further suggested that the three detected runaway stars might only represent about one fifth of the ejected O stars. This would imply that NGC 6611 already displays a significant dynamical evolution. We emphasize that the present work only addresses the multiplicity properties of the current O-type star population in NGC 6611.

This work is organised as follows. Sect. 2 describes our observing campaign and the data reduction process. Sect. 3 revises the properties of the individual O-type stars in the cluster. Sect. 4 presents an analysis of the observational biases using Monte-Carlo simulations. Finally, Sect. 5 discusses the present results and Sect. 6 summarizes our conclusions.

2 OBSERVATIONS AND DATA HANDLING

The core of our data set is formed by 66 high-resolution FEROS spectra obtained from May 2004 to June 2006 at the ESO/MPG-2.2m telescope at La Silla (PI: Sana). The FEROS spectrograph provides us with the complete optical spectrum (3800-9200 Å) at once, with a spectral resolving power of 48 000. The FEROS properties are identical to those given in Paper I, and the data reduction process is described in detail in Sana (2009). Exposure times ranged between 10 and 45 min depending on the object magnitude, yielding a typical signal-to-noise ratio (SNR) of 200 as measured in the continuum close to 5000 Å.

A second part of our data set is composed of 10 FLAMES-GIRAFFE spectra, five FEROS spectra and six FLAMES-UVES spectra from the VLT-FLAMES survey of massive stars (PI: Smartt). Those data and the data reduction have been previously described by Evans et al. (2005). Additionally, we retrieved one FEROS spectrum of HD 168075 and one of HD 168076 (PI: Bouret) from the ESO archive. We also retrieved three UVES long-slit echelle spectra of HD 168076 (PI: Andre). The two FEROS spectra were reduced as described above while the UVES data were reduced using the ESO CPL-based pipeline and normalised by fitting low-order polynomials to the continuum of the individual orders. Finally, five objects were re-observed with FEROS in

Table 3. Journal of the spectroscopic observations of the O-type stars in NGC 6611. First and second lines indicate the spectral line and the adopted rest wavelength (in Å). The first column gives the heliocentric Julian date at mid-exposure. The following columns provide, for each spectral line, the measured RVs (in km s^{-1}). References for the instrumental setup can be found at the bottom of the table. The full table is available in the electronic edition of the journal.

HJD	He I $\lambda 4026$	Si IV $\lambda 4089$	He I $\lambda 4144$	He I $\lambda 4388$	He I $\lambda 4471$	Mg II $\lambda 4481$	He II $\lambda 4542$	He II $\lambda 4686$	He I $\lambda 4922$	He II $\lambda 5412$	He I $\lambda 5876$	He I $\lambda 7065$
-2 400 000	4026.072	4088.863	4143.759	4387.928	4471.512	4481.228	4541.590	4685.682	4921.929	5411.520	5875.620	7065.190
BD-13° 4923 prim												
52836.70812 ^d	-	-	82.4	-	62.7	55.1	68.6	91.7	-	-	-	-
52839.75137 ^d	-	-	-	-	60.5	52.6	75.2	92.2	-	-	-	-
53134.95474 ^e	-	-	-	-	-	-	-	11.2	-	11.3	42.0	-
53509.84538 ^a	-79.4	-	-	-	-63.7	-	-64.4	-56.3	-	-63.8	-70.5	-
53510.87032 ^a	-	-	-	-	-	-	-4.1	-11.5	-	-0.2	24.6	-
53511.76887 ^a	-	-	-	-	-	-	18.2	25.0	-	18.4	-2.9	-
53512.75277 ^a	-	-	-	-	47.3	44.6	35.6	49.9	-	37.9	54.9	-
53860.83796 ^a	80.7	-	-	-	58.8	-	69.0	81.9	-	70.3	62.2	-
53861.72041 ^a	-	-	31.8	-	43.4	56.1	39.1	78.7	49.7	41.3	56.2	-
53862.72524 ^a	-	-	22.0	-	-	46.2	27.5	59.5	-	27.2	42.7	-
53863.84924 ^a	-	-	-	-	-	-	16.3	42.2	-	14.2	6.3	-
53864.75611 ^a	-	-	-	-	-	-43.6	-3.5	24.9	-52.7	-2.1	17.8	-
BD-13° 4923 sec												
52836.70812 ^d	-21.1	-85.5	-83.0	-79.8	-86.0	-88.3	-126.1	-80.5	-	-	-	-
52839.75137 ^d	-	-	-	-81.5	-86.3	-89.1	-101.5	-76.6	-	-	-	-
53134.95474 ^e	-	-	-	-	-	-	-	-	-	-	-50.6	-
53509.84538 ^a	161.0	157.8	149.1	56.0	152.3	142.0	164.0	158.3	149.8	174.8	153.9	53.2
53510.87032 ^a	4.3	63.5	64.2	60.9	15.1	-	-	49.9	55.2	-	-	-9.6
53511.76887 ^a	-9.1	-21.5	-27.6	-23.1	-12.2	-14.3	-	-11.5	-19.6	-	-	-9.6
53512.75277 ^a	-27.0	-69.3	-73.9	-68.5	-74.2	-81.1	-	-82.5	-70.8	-	-71.7	71.5
53860.83796 ^a	-85.0	-93.0	-	-97.7	-101.5	-102.1	-139.1	-95.8	-96.7	-115.1	-96.1	99.3
53861.72041 ^a	-19.9	-79.2	-80.9	-74.3	-88.9	-84.4	-	-88.3	-81.1	-	-77.1	79.5
53862.72524 ^a	-13.5	-49.1	-50.3	-46.0	-32.8	-50.9	-	-67.2	-44.4	-	-46.4	44.4
53863.84924 ^a	-6.7	3.6	5.5	-2.6	2.9	-1.7	-	-32.6	3.4	-	-	6.6
53864.75611 ^a	-0.1	62.5	56.3	58.0	16.4	46.7	-	-	57.9	-	-	54.1

a. ESO2.2m + FEROS ; b. VLT + UVES; c. VLT + FLAMES-UVES; d. VLT + FLAMES-GIRAFFE; e. WHT + ISIS

Table 4. Diagnostic line ratios and corresponding spectral types for the O-type objects studied. *n/a* indicates criteria that either do not apply to the considered spectral type or for which the lines could not be securely measured and/or separated. We refer to text for discussion of the individual cases and to Table 9 for the finally adopted spectral types. The error-bars give the 1- σ dispersions on the measurements.

Object	Component	$\log W'$	$\log W''$	$\log W_{\lambda 4686}$	$\log W'''$	Sp. Type
BD-13°4923	Primary	-0.612 ± 0.130	<i>n/a</i>	$> 2.751 \pm 0.071$	<i>n/a</i>	O4 V((f))
BD-13°4923	Secondary	0.125 ± 0.063	<i>n/a</i>	$> 2.147 \pm 0.182$	<i>n/a</i>	O7.5 V
BD-13°4927	<i>n/a</i>	-0.020 ± 0.014	<i>n/a</i>	2.348 ± 0.041	<i>n/a</i>	O7 III(f)
BD-13°4928	<i>n/a</i>	0.541 ± 0.057	0.147 ± 0.151	<i>n/a</i>	5.531 ± 0.109	O9.5 V
BD-13°4929	Primary	-0.044 ± 0.086	<i>n/a</i>	$> 2.637 \pm 0.063$	<i>n/a</i>	O7 V
BD-13°4930	<i>n/a</i>	0.272 ± 0.066	-0.299 ± 0.021	<i>n/a</i>	5.333 ± 0.009	O8.5 V
HD 168075	Primary	-0.096 ± 0.030	<i>n/a</i>	$> 2.837 \pm 0.012$	<i>n/a</i>	O6.5 V((f))
HD 168076	Composite	-0.721 ± 0.061	<i>n/a</i>	<i>n/a</i>	<i>n/a</i>	O4 V((f))
HD 168137	Primary	-0.075 ± 0.039	<i>n/a</i>	$> 2.644 \pm 0.033$	<i>n/a</i>	O6.5 V
HD 168137	Secondary	0.202 ± 0.068	<i>n/a</i>	$> 2.598 \pm 0.046$	<i>n/a</i>	O8 V
HD 168183	Primary	0.608 ± 0.026	0.034 ± 0.031	<i>n/a</i>	$> 5.270 \pm 0.021$	O9.5 III

Table 5. Cross-identification and physical properties of the O-type stars in NGC 6611. The magnitudes are from Guarcello et al. (2007), except for the two brightest objects for which data from Hillenbrand et al. (1993) are quoted. The stellar parameters come from Dufton et al. (2006). The uncertainties are the 1- σ error-bars quoted by the authors.

HD	BD	Walker	ESL05	GPM07	V	$B - V$	T_{eff} (kK)	$\log g$ (cm s^{-2})	$\log L$ (L_{\odot})	$v \sin i$ (km s^{-1})
168183 ^a	-13°4991	W412	6611-001	24374	8.18	0.34	32.0	3.60	5.39	142
168076 ^a	-13°4926	W205	6611-002	27436	8.18	0.43	41.5	3.90	5.86	102
168075 ^a	-13°4925	W197	6611-003	18360	8.752 ± 0.037	0.543 ± 0.107	40.0	3.90	5.63	87
168137 ^a	-13°4932	W401	6611-004	13706	8.942 ± 0.006	0.407 ± 0.025	37.0	4.00	4.85	76
-	-13°4930 ^b	W367	6611-006	13867	9.368 ± 0.023	0.343 ± 0.079	34.0	4.10	4.84	43
-	-	-	-	-	-	-	31.3	4.00	4.81	20
-	-13°4927	W246	6611-008	6835	11.114 ± 0.541^c	0.669 ± 0.607	36.0	3.50	5.75	100
-	-13°4929 ^a	W314	6611-011	19208	9.803 ± 0.203	0.706 ± 0.208	36.0	4.20	5.24	66
-	-13°4923	W175	6611-014	5890	10.007 ± 0.011	0.979 ± 0.019	-	-	-	-
-	-13°4928	W280	6611-015	1806	10.044 ± 0.039	0.560 ± 0.048	32.5	3.90	4.77	410
-	-	W166	6611-017	18715	10.296 ± 0.003	0.728 ± 0.010	36.0	3.95	5.02	95
-	-	W161	6611-029	5818	11.215 ± 0.007	1.241 ± 0.008	36.0	3.85	5.37	135
-	-	W584	6611-045	5510	12.052 ± 0.008	1.235 ± 0.010	35.0	4.00	5.04	25
-	-	W222	6611-080	3820	12.968 ± 0.008	1.519 ± 0.009	40.0	4.00	5.33	95

a. For those objects, the composite nature of their spectrum was not known, thus not taken into account while deriving the stellar parameters. The latter might thus be indicative only.

b. The entries on the second row quote the results obtained by Hunter et al. (2007), who re-analysed the BD-13°4930 spectrum and obtained slightly different stellar parameters.

c. Hillenbrand et al. (1993) quote $V = 9.46$, suggesting that BD-13°4923 is brighter than reported by Guarcello et al. (2007), although marginally in agreement within the (rather large) error-bars from the latter.

March 2009 (PI: Evans) to improve the detection likelihood of long-period systems. These additional data were reduced as described above and have a typical SNR of 250 to 300 at 5000 Å. Table 1 gives a brief overview of the wavelength coverage and spectral resolution of the different spectra in our data set.

Using the reduced spectra, Doppler shifts and equivalent widths (EWs) were measured by simultaneously fitting one to three Gaussians (depending on whether an SB1, SB2 or SB3 signature was visible) to a series of line profiles (Table 2). Effective rest wavelengths were taken from Conti et al. (1977) and from Underhill (1994) for lines below and above 4800 Å, respectively, to compute the radial velocities (RVs). Table 3 provides the journal of the observations and lists, for each spectral line, the measured RVs.

The achieved RV accuracy is strongly dependent on the

width of the lines, thus on the projected rotation rate of the star. Using a purely empirical approach, Fig. 17 in this work and Fig. 10 in Paper I provide us with the following guidelines. For slow rotators ($v \sin i < 50 \text{ km s}^{-1}$), an rms accuracy of 1 km s^{-1} or better can be achieved. For more typical rotation rates ($v \sin i \sim 100\text{-}200 \text{ km s}^{-1}$), typical dispersions in the measured velocities are between 2 and 5 km s^{-1} . For fast rotators ($v \sin i > 300 \text{ km s}^{-1}$), the precision of the measurements drops significantly, with rms dispersions close to 15 km s^{-1} .

As in Paper I, the spectral classification is based on the quantitative criteria of Conti & Alschuler (1971), Conti (1973), Mathys (1988) and Mathys (1989), that rely on the EWs of given diagnostic lines. We adopt the following notations: $\log W' = \log W(\lambda 4471) - \log W(\lambda 4542)$, $\log W'' = \log W(\lambda 4089) - \log W(\lambda 4144)$ and $\log W''' =$

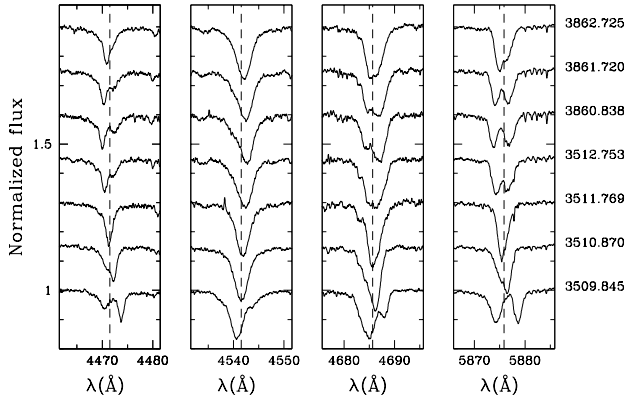


Figure 1. BD-13°4923: He I $\lambda\lambda 4471$, 5876 and He II $\lambda\lambda 4542$, 4686 line profiles at different epochs. The heliocentric Julian dates at mid-exposure are given at right-hand in format HJD-2450000. The spectra have been shifted along the y -axis for clarity. The vertical dashed lines indicate the adopted rest-wavelength for each spectral line.

Table 6. BD-13°4923: best-fit orbital solutions using the data set from the present work alone or combined with the Bosch et al. RV measurements (primary only). T (in HJD-2450000) is the time of periastron passage and is adopted as phase $\phi = 0.0$ in Fig. 3. Quoted uncertainties correspond to 1- σ error-bars.

Parameter	This work	Combined
P (d)	13.2722 ± 0.0027	13.2677 ± 0.0007
e	0.285 ± 0.030	0.302 ± 0.045
ω ($^\circ$)	199.3 ± 9.5	188.5 ± 9.8
T	2995.491 ± 10.144	3005.016 ± 0.376
γ_1 (km s^{-1})	30.7 ± 4.3	28.7 ± 4.6
γ_2 (km s^{-1})	3.4 ± 5.3	7.5 ± 6.0
K_1 (km s^{-1})	81.0 ± 5.3	82.6 ± 7.0
K_2 (km s^{-1})	140.2 ± 9.2	142.8 ± 12.2
$q = M_2/M_1$	0.578 ± 0.043	0.578 ± 0.043
$M_1 \sin^3 i$ (M_\odot)	8.3 ± 1.5	8.6 ± 2.1
$M_2 \sin^3 i$ (M_\odot)	4.8 ± 0.8	5.0 ± 1.2
rms (km s^{-1})	7.9	12.9

$\log W(\lambda 4388) + \log W(\lambda 4686)$, where the EWs are expressed in mÅ. The first criterion, $\log W'$ can be used across the entire O-type range. $\log W''$ and $\log W'''$ are restricted to stars strictly later than O6 and O8, respectively, while $\log W_{\lambda 4686}$ can be used for O8 stars and earlier. The measurements and the corresponding spectral types are given in Table 4 and discussed in Sect. 3. Measured EWs for binary components only provide a lower limit on the real strength of the lines. This affects the latter two criteria, so that the values quoted in Table 4 for $\log W'''$ and $\log W_{\lambda 4686}$ are only lower limits.

3 O-TYPE STARS IN NGC 6611

This section briefly discusses the data associated with each O-type object in our sample, with a particular emphasis on the spectral properties and on the multiplicity status. As mentioned earlier, NGC 6611 hosts 13 O-type stars. Table 5 provides the cross-identification between HD/BD numbers

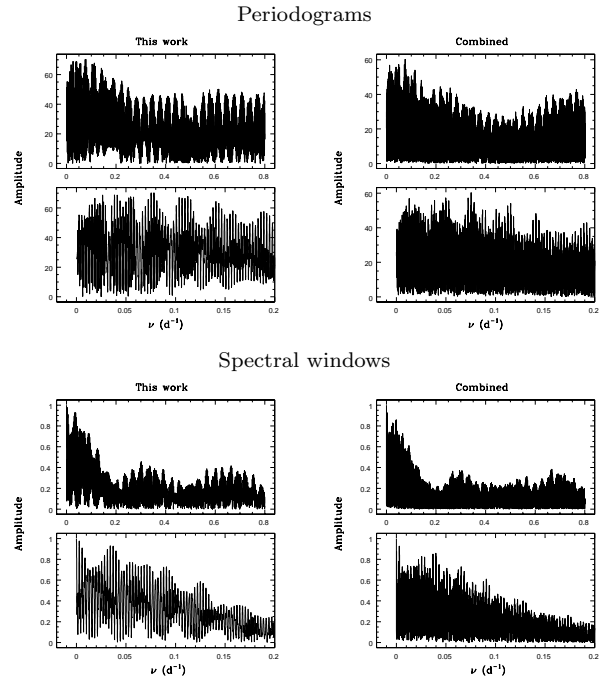


Figure 2. BD-13°4923: periodograms (upper row) and spectral windows (lower row) computed using the data from this work alone (left-hand column) or combined with the Bosch et al. measurements (right-hand column).

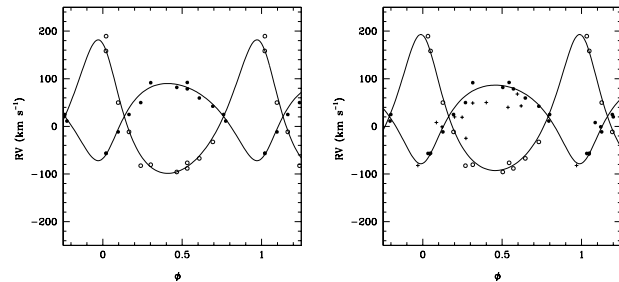


Figure 3. BD-13°4923: RV-curves corresponding to the orbital solutions of Table 6. *Left:* using data from this work. *Right:* combined with the Bosch et al. measurements. Filled and open symbols indicate the primary and secondary RV measurements from this work while crosses give the primary RVs from Bosch et al.

and the numeration of Walker (1961), Evans et al. (2005, ESL05) and Guarcello et al. (2007, GPM07). It also lists the stellar parameters obtained by Dufton et al. (2006) from atmosphere model fitting. The four faintest O-stars were not re-observed as part of our monitoring program, so that only one or two spectra are available for each object. Those four stars are thus omitted in the rest of this paper.

This section is organised as follows. We first present the gravitationally-bound systems (Sect. 3.1). In Sect. 3.2, we discuss objects whose spectra most likely present multiple signatures, although our current data set does not allow us to conclude whether the different components are gravitationally-bound or arise from spurious alignment. Fi-

nally, Sect. 3.3 summarizes the properties of the remaining, presumably single, O-type stars.

3.1 Gravitationally-bound systems

3.1.1 *BD-13°4923 (W175)*

Classified as O5 V((f*)) by Hillenbrand et al. (1993), BD-13°4923 was first suspected to be an O+O binary with a period larger than eight days by Bosch et al. (1999). Based on the fact that the He I and He II lines were moving in the opposite direction, these authors suggested that the primary was an early O star and the secondary, a late one, a fact later confirmed by Evans et al. (2005). Duchêne et al. (2001) further reported a low-mass visual companion at $0.67''$ (≈ 1200 A.U.), with an estimated mass between 2 and $4 M_{\odot}$.

We collected 10 additional spectra over three years. At least four of them clearly show the signatures of the two components both in the He I and He II lines (Fig. 1), allowing us to put additional constraints on the orbital and physical properties of the components. Using the well-separated spectra only, we refined the spectral classification to O4 V((f))+O7.5 V with, respectively, the O5 and O7 spectral sub-type at $1-\sigma$. The third, more distant, component is likely a late-B/early-A star. It is thus expected to contribute to less than 1% of the total continuum level and will not affect the RV and EW measurements of the two O stars. It has thus been neglected in the present analysis.

Because we only have a limited data set, we also made use of previously discarded data. First, one of our FEROS spectra was obtained late during morning twilight and is contaminated by the solar spectrum. From He II $\lambda 4686$ and redward, the solar and stellar spectra can however be easily separated, allowing us to recover most of the prominent stellar lines in that region. Second, the WHT-ISIS spectrum from Evans et al. (2005) exhibits a clear wavelength calibration shift in the $\lambda 4800$ Å setting. To solve this issue, we have cross-calibrated the ISIS wavelength solution with respect to our own data, by using the narrow DIBs at $\lambda\lambda 4763$, 4780 and 4964 (Hobbs et al. 2008). This allowed us to achieve a corrected wavelength calibration with an rms dispersion better than 0.1 Å (~ 5 km s $^{-1}$), sufficient thus for our purpose.

In the following, we focus explicitly on the He II $\lambda 4686$ line which is the only strong SB2 line common to all our spectra. To improve the disentangling of heavily blended profiles, we adopted the line shapes as determined on widely separated spectra obtained during the same run, thus fitting the Doppler shifts only. Although it is not clear whether our data cover any of the extrema of the RV-curve, we attempted to constrain the orbital period using the Fourier method of Heck et al. (1985), as revisited by Gosset et al. (2001). The obtained periodogram shows two dominant peaks at $\nu \approx 0.075$ and 0.078 d $^{-1}$ (Fig. 2). Including the He II measurements of Bosch et al. (1999) further allows us to determine that the signal at $\nu \approx 0.075$ d $^{-1}$ is most likely to correspond to the true periodicity of the orbit.

Using the corresponding period $P \approx 13.2679$ d as a first guess, we used the Liège Orbital Solution Package (LOSP, Sana & Gosset 2009) to compute a preliminary SB2 orbital solution. Table 6 and Fig. 3 respectively give the best-fit or-

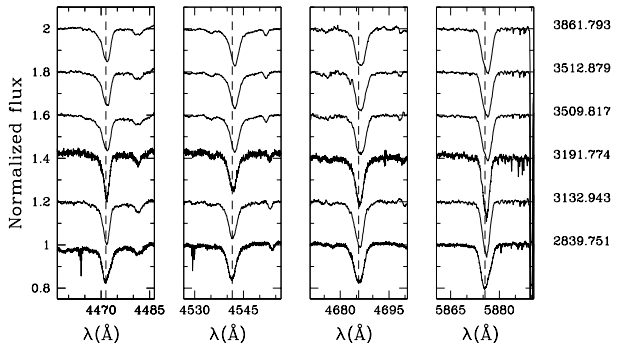


Figure 4. HD 168075: He I $\lambda\lambda 4471$, 5876 and He II $\lambda\lambda 4542$, 4686 line profiles at different epochs. Note the changing asymmetry of the He I lines.

bit parameters and the corresponding RV-curves. We note that the period uncertainties given in Table 6 only refer to the fitted models. As such, they do not account for the presence of multiple peaks in the periodogram. Both solutions, computed with and without including literature data, are in good agreement although Fig. 3 reveals some systematic deviations between the best fit solution and the RV points of Bosch et al. (1999). Yet, the latter measurements might suffer from significant systematic errors because the SB2 signature was not separated. With $e \approx 0.3$, the obtained solution is significantly eccentric. The derived mass-ratio is in perfect agreement with the estimated spectral types of the components. Given the computed minimal masses, one would predict an orbital inclination about 30 to 40° , so that no eclipses are expected.

3.1.2 *HD 168075 (W197)*

So far classified as an O6-O7 V((f)) star (Evans et al. 2005), HD 168075 was first suggested to be a binary by Conti et al. (1977). Later on, Bosch et al. (1999) reported no short-term variations but mentioned significant changes in data taken two years apart. These authors further reported the detection of Si III, N III and O II absorption lines normally not present in a typical O7 spectrum.

Our data sample, formed by about 10 spectra collected over three years, confirms this object is a long period binary. As found by Bosch et al., we clearly detect Si III, N III and O II lines in absorption, whose motion is anti-correlated with the He I and He II line motion, thus confirming their association with the secondary star. As observed in Fig. 4, the He I $\lambda 4471$ and He II $\lambda 4686$ lines display clear profile changes, likely due to the blending of the primary and secondary signatures, while the He II $\lambda 4542$ line profile seems to remain constant in shape. This strongly suggests the secondary to be a B0-B1 star. Using the He I $\lambda 4471$ over He II $\lambda 4542$ EW ratio, we adopt a O6.5 V((f)) spectral type for the primary, with a O7 sub-type well within $1-\sigma$. We finally note that the He I $\lambda 4471$ line EW might have been overestimated because of the secondary blend, so that the primary could be slightly hotter than the adopted spectral sub-type.

Our data alone do not allow us to definitely constrain the orbital properties of HD 168075. Using a much larger data set, Barbá et al. (2009) recently proposed a prelimi-

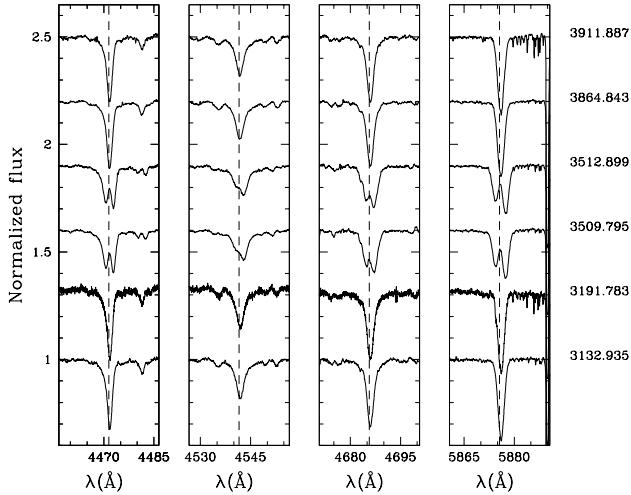


Figure 5. HD 168137: He I $\lambda\lambda 4471, 5876$ and He II $\lambda\lambda 4542, 4686$ line profiles at different epochs. Note the clear SB2 signature at HJD–2 450 000 \sim 3509.8 and 3512.9.

nary orbital solution, with a period of 43.6 d and a slightly eccentric orbit $e = 0.17$. They independently confirmed the O6.5 V((f)) classification for the primary and proposed that the secondary is a B0.2 III star.

3.1.3 HD 168137 (W401)

HD 168137 is known as an O8.5 V isolated star. Between May 2004 and May 2006, we acquired 10 FEROS spectra and, in March 2009, we obtained one additional FEROS observation. Our prime data set is completed by one GIRAFFE spectrum and one UVES spectrum from Evans et al. (2005) obtained in 2003. While our May 2004, 2006 and 2009 observations are very similar to the spectra of Evans et al., the May 2005 data reveal a clear SB2 signature (Fig. 5). No further RV variations could be detected within the 2005 campaign. Similarly, no variations are seen between the May and June 2006 spectra, suggesting a period larger than 30 days. Using the well-separated spectra only, we revise the spectral classification to O7 V+O8 V, with the O6.5 and O7.5 subclasses at $1-\sigma$ respectively for the primary and secondary components. A long term monitoring is required to bring further constraints on the orbital properties of this system.

3.1.4 HD 168183 (W412)

At $\sim 13'$ SE of the center of the cluster, HD 168183 is a known SB1 eclipsing binary with a period close to 4 d (Hipparcos Catalogue 1997; Bosch et al. 1999). The object has been classified O9.5 I by Hillenbrand et al. (1993) and Bosch et al. (1999), and B0 III by Evans et al. (2005). With a significant He II $\lambda 4542$ line in absorption, HD 168183 cannot be a B star. Indeed the EW ratio of He I $\lambda 4471$ to He II $\lambda 4542$ points to an O9.5 spectral type. With He I $\lambda 4144$ only slightly shallower than Si IV $\lambda 4089$, plus He II $\lambda 4686$ and H α in absorption, the properties of the spectrum of HD 168183 are definitely not those of a supergiant. Given

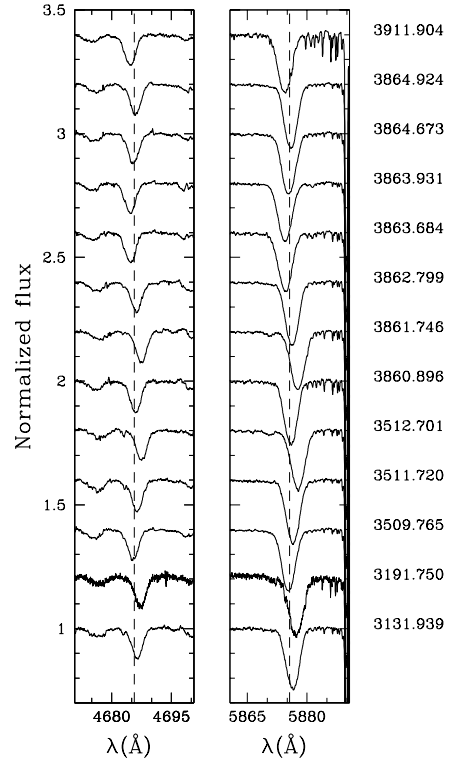


Figure 6. HD 168183: He II $\lambda 4686$ and He II $\lambda 5876$ line profiles at different epochs. Note the faint SB2 signature at HJD–2 450 000 \sim 3512.7 and 3861.7.

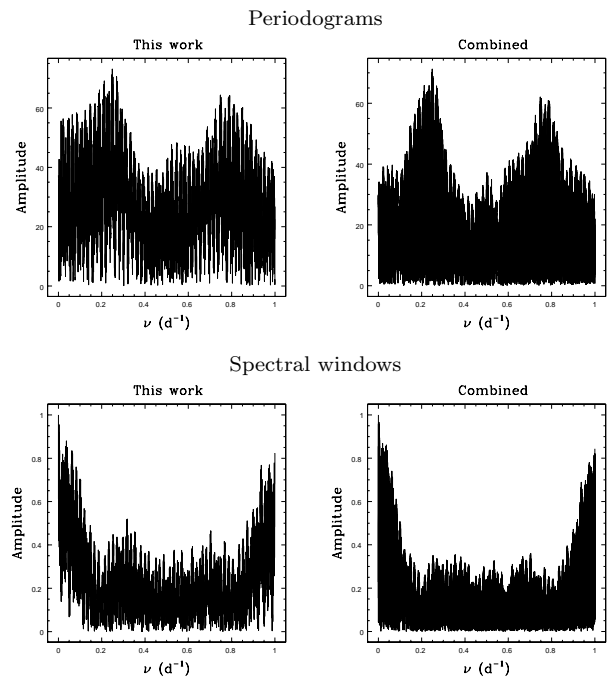


Figure 7. HD 168183: periodograms (upper row) and spectral windows (lower row) computed using the He I data from this work alone (left-hand column) or combined with the Bosch et al. measurements (right-hand column).

Table 7. HD 168183: orbital solutions obtained using different data sets: the RVs of the He I $\lambda 5876$ line (Col. 2), the average of the He I measurements (Col. 3) and the average of the He I measurements combined with the Bosch et al. data (Col. 4). The usual notations have been used. T (in HJD-2 450 000) is the time of periastron passage and is adopted as phase $\phi = 0.0$ in Fig. 8. Quoted uncertainties correspond to 1- σ error-bars.

	He I $\lambda 5876$ line	He I line	Combined
P (d)	4.01554 ± 0.00017	4.01556 ± 0.00015	4.015575 ± 0.000022
e	0.039 ± 0.015	0.052 ± 0.014	0.059 ± 0.015
γ (km s^{-1})	19.2 ± 1.0	19.3 ± 0.9	18.5 ± 0.8
K (km s^{-1})	83.9 ± 1.5	78.5 ± 1.3	77.8 ± 1.3
T	2998.718 ± 0.388	2998.786 ± 0.244	2998.881 ± 0.195
ω ($^\circ$)	13.9 ± 35.8	20.1 ± 22.7	28.9 ± 17.5
f_{mass}	0.245 ± 0.013	0.200 ± 0.010	0.195 ± 0.009
rms (km s^{-1})	3.3	2.8	3.7

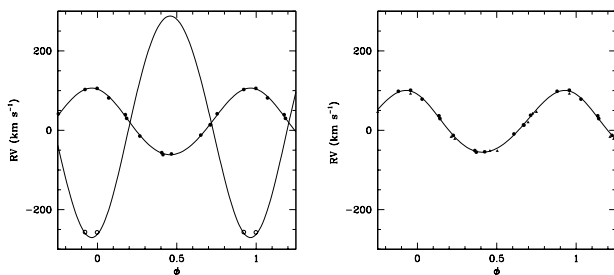


Figure 8. HD 168183: RV-curves corresponding to orbital solutions of Table 7, based on the He I $\lambda 5876$ line data set (left) and on the average of the He I line RVs combined with Bosch et al. measurements (right). Filled and open circles show primary and secondary RV measurements from this work while filled triangles show the Bosch et al. data.

the brightness of HD 168183, we finally adopt a O9.5 III spectral classification for the primary.

Thanks to their high SNR, our data reveal the secondary signature for the first time. Though faint, the secondary spectrum is indeed clearly visible in the He I $\lambda 5876$ line, as a broad and very shallow component, peaking at $\approx 2\%$ of the continuum level (Fig. 6). Because of the large difference in the line EWs (a factor ~ 20 for He I $\lambda 5876$), indicating a significant difference in flux, and because we could not detect the secondary signature in the He II lines, we suggest that the secondary is a mid-B type star.

As for BD-13 $^\circ$ 4923, we used the Fourier technique of Heck et al. (1985) and Gosset et al. (2001) to estimate the orbital period of the system. Resulting periodograms are shown in Fig. 7 and present a clear peak at $\nu \approx 0.25 \text{ d}^{-1}$. Using LOSP, we first computed the primary orbital solution. Significantly better residuals are obtained using a limited eccentricity compared to a circular solution. We derived a RV-curve semi-amplitude K_1 and a mass function f_{mass} larger than those proposed by Bosch et al. (1999). Combining our data with theirs yields essentially the same best-fit solution (Table 7).

Assuming that the primary orbital solution is correct and that both components share the same systemic velocity, it is in principle possible to constrain the secondary orbit with a single RV measurement. For the purpose of this exercise, we adopt the He I $\lambda 5876$ orbital solution of

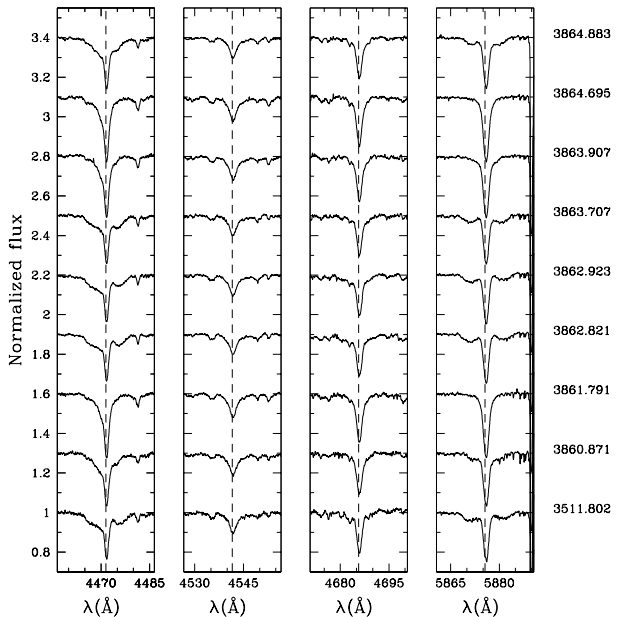


Figure 9. BD-13 $^\circ$ 4929: He I $\lambda\lambda 4471, 5876$ and He II $\lambda\lambda 4542, 4686$ line profiles at different epochs. The close B+B pair signature is clearly visible in the He I lines at HJD-2 450 000 from 3862.8 to 3863.7.

Table 7, propagating the uncertainties on the primary parameters at the first order by means of the theory of error propagation (Bevington 1969). Using the two observations where the SB2 signature is well seen, we estimate $K_2 = 279.1 \pm 10.9 \text{ km s}^{-1}$. This yields $q = M_2/M_1 = 0.301 \pm 0.013$, $M_1 \sin^3 i = 15.3 \pm 1.9 M_\odot$ and $M_2 \sin^3 i = 4.6 \pm 0.4 M_\odot$. The corresponding RV-curves are displayed in Fig. 8. While this result supposes that the adopted time series alias corresponds to the true period, we note that the obtained mass ratio is in good agreement with the component spectral types as previously discussed. Under such assumption, the orbital inclination would be $i \approx 65^\circ$, compatible with the presence of eclipses as detected by HIPPARCOS.

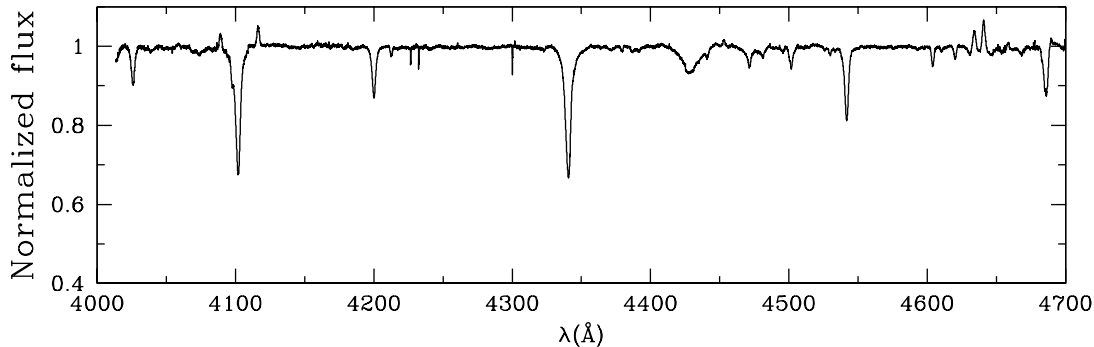


Figure 10. HD 168076: spectrum in the range 4000-4700 Å. Note the Si IV $\lambda\lambda$ 4089-4116 and N III $\lambda\lambda$ 4634-4640-4642 lines in emission and the N V $\lambda\lambda$ 4604-4620 absorption.

3.2 Composite systems

3.2.1 *BD-13°4929 (W314)*

Classified B0 V by Hillenbrand et al. (1993) and Bosch et al. (1999), the star’s spectral type was revised to O9 V by Evans et al. (2005). The latter authors further noticed slight profile asymmetries, suggesting that BD-13°4929 is an SB2 binary system. Our new data allow us to shed new light on the nature of BD-13°4929. From Fig. 9, it is obvious that BD-13°4929 is an SB3 system, formed by a short-period binary with nearly identical early B companions displaying broad and shallow lines, and a third O-type star. Because the O star has much sharper line profiles, it is easily disentangled from the close B+B pair using multi-Gaussian profile fitting. Based on the He I λ 4471 to He II λ 4542 line ratio, we assign the O star an O7 spectral sub-type, with the O7.5 type at $1-\sigma$. With no sign of emission lines plus the fact that the observed (diluted) EW of the He II λ 4686 is $\log W_{\lambda 4686} = 2.64 \pm 0.06$ (mÅ), we confirm the dwarf luminosity class. The signatures of the fainter companions are not visible in the He II λ 4542 line, but show a faint contribution to He II λ 4686. We thus adopt a B0.5 spectral sub-type for both companions of the O star. Given the object magnitude, we consider that the B+B pair is also formed by two dwarfs. While in reality the two B stars are not exactly identical as indicated by slight differences in their EWs (Fig. 9), more data would be needed to refine the classification further.

The B+B binary has a probable period close to 4 d, but our data do not allow us to put quantitative constraints on the orbit of the tight system. Similarly, the O-type component does not show any significant RV variations and we cannot decide whether the O star is gravitationally linked to the B+B pair or not. We however note that the chance of spurious alignment of an O and a B star in NGC 6611 is very small. BD-13°4929 is thus an excellent candidate of hierarchical triple system formed by a close B0.5 V+B0.5 V pair plus a wider O7 V companion.

3.2.2 *HD 168076 (W205)*

Close to the cluster centre, HD 168076 is the brightest optical source in NGC 6611. Reported as an SB candidate by Conti et al. (1977) based on two discrepant RV points, further investigations by Bosch et al. (1999) could not confirm its binary nature. We collected only a few spectra in 2006

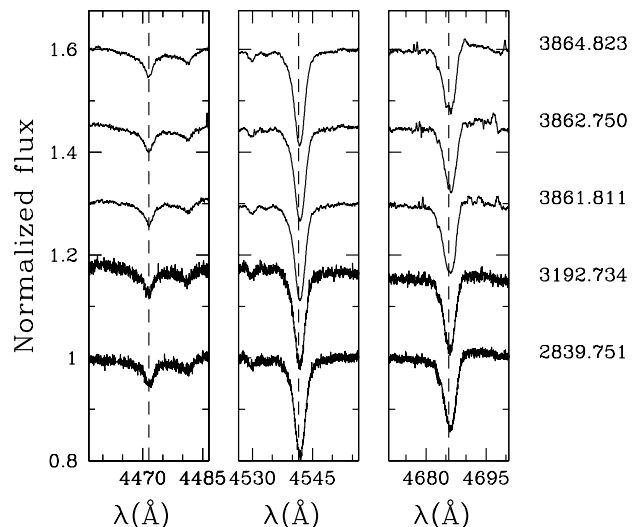


Figure 11. HD 168076: He I λ 4471 and He II $\lambda\lambda$ 4542, 4686 line profiles at different epochs.

that show no variability, neither on short time scales nor, by comparison with similar quality data from Evans et al. (2005) and from May 2009, on longer time scales (Fig. 11). The EW ratio of the He I λ 4471 and He II λ 4542 lines and the presence of He II λ 4686 strongly in absorption point towards an O4 V((f)) classification, as previously adopted by various authors.

Bosch et al. (1999) however reported a relatively bright companion at $0.15''$ from HD 168076. Given the aperture on the sky of the FEROS fibre ($\varnothing = 2.0''$), the spectrograph thus provides us with a blended spectrum of the two stars and the classification criteria used so far are not applicable. In a second approach, we used the O2-O4 spectroscopic atlas of Walborn et al. (2002) to refine the spectral classification of HD 168076. Because of the presence of N V in absorption and of Si IV in emission with moderate strength, but no N IV λ 4058 (Fig. 10), the spectrum of HD 168076 looks very much like the one of HD 93128 and we thus adopt an O3.5 V((f+)) spectral classification for the earliest object of the pair.

Dufton et al. (2006) reported masses of 38 and 16 for both objects, which is likely to have been underestimated

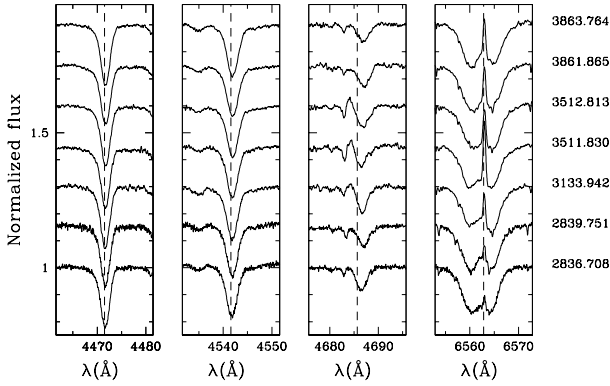


Figure 12. *BD-13°4927*: He I $\lambda\lambda 4471$, He II $\lambda\lambda 4542$, 4686 and H α line profiles at different epochs. Note the variable emission that partially fills the He II $\lambda 4686$ and H α lines.

given that a typical O3.5 V star is about $52 M_{\odot}$ (Martins et al. 2005). Assuming that the quoted mass ratio ($q = 0.42$) is correct, the secondary component could be an O7.5 V or an O9 III. The expected luminosity ratio would correspond to 5 and 3.5 respectively, which is sufficient in both cases to significantly affect the apparent He I to He II line ratio in the composite spectrum. Because it is unlikely that the secondary evolved more quickly than the primary and because previous mass-transfer episode appears very unlikely in such a young cluster, we finally adopt the O7.5 V classification for the secondary. Under these assumptions, and given the measured angular separation from Bosch et al. (1999), we estimate a minimal orbital period of several hundreds of years.

3.3 Presumably single stars

3.3.1 *BD-13°4927 (W246)*

Reported as O7 II(f) by Hillenbrand et al. (1993), no significant RV variation was detected by Bosch et al. (1999). We collected five FEROS spectra from 2004 to 2006, plus one spectrum in 2009, and we further included GIRAFFE data from 2007 in our analysis. With $W_{\lambda 4471} \approx W_{\lambda 4542}$, this object is definitely an O7 star. Small RV variations ($\sim 10 \text{ km s}^{-1}$ peak-to-peak) are detected, although at the limit of significance, and can easily be mimicked by low-amplitude wind effects. Because $\log W_{\lambda 4686} < 2.75$ (mÅ) and because He II $\lambda 4686$ and H α are partly filled with emission (Fig. 12), the adopted spectroscopic criteria indicate a giant luminosity class. Yet, with N III $\lambda\lambda 4634-40-42$ in emission, the spectrum of *BD-13°4927* is much more alike HD 151515 (O7 II(f)) than HD 93522 (O7 III(f)). Combined with the fact that *BD-13°4927* displays a magnitude midway between O7 III and O7 I typical objects (Martins et al. 2005), we confirm the O7 II(f) spectral classification. From our campaign, the star is likely to be single.

3.3.2 *BD-13°4928 (W280)*

Located close to the cluster centre, *BD-13°4928* was reported as a single O9.5 V star by Bosch et al. (1999). We obtained seven additional FEROS spectra that revealed rotationally broadened lines (Fig. 13). Because of this, very few

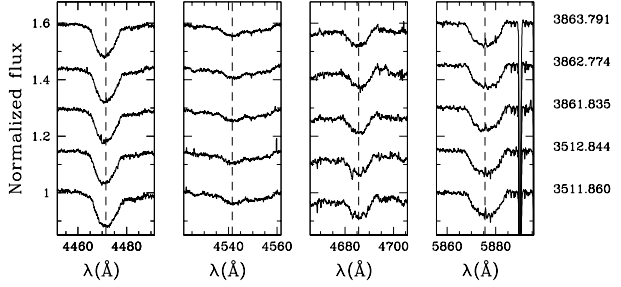


Figure 13. *BD-13°4928*: He I $\lambda\lambda 4471$, 5876 and He II $\lambda\lambda 4542$, 4686 line profiles at different epochs. Note the shallow He II $\lambda 4542$ line.

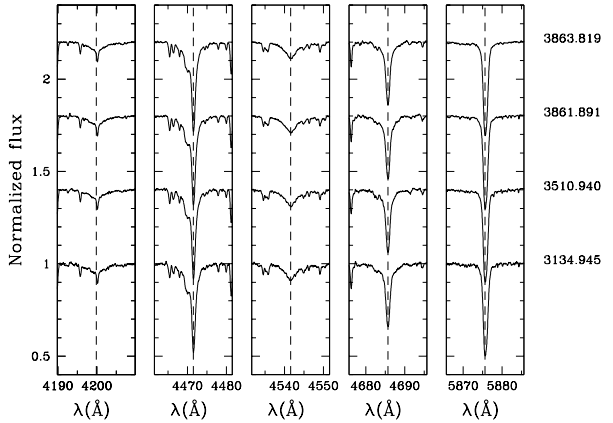


Figure 14. *BD-13°4930*: He I $\lambda\lambda 4471$, 5876 and He II $\lambda\lambda 4200$, 4542, 4686 line profiles at different epochs.

continuum windows were available in the $\lambda\lambda 4050-4700 \text{ \AA}$ region of the spectrum. In this range, we used the spectra obtained just before or just after those of *BD-13°4928* to empirically correct for the instrument response curve. Using this approach, we routinely achieved a precision better than half a percent of the continuum in the response curve correction, only leaving a residual slope in the *BD-13°4928* spectrum. The latter slope, due to the difference of effective temperature between the two objects, was finally removed by fitting a low order polynomial to the continuum of the pre-normalised spectra.

Minor line profile variations seem to be present but can originate from the object’s rapid rotation. Because the lines are rotationally broadened, their profiles deviate significantly from a Gaussian shape. In the present case, we used a rotation profile to measure the Doppler shifts, fitting simultaneously the line centre, its amplitude and the star’s projected rotational velocity $v \sin i$. The RVs obtained show a rms dispersion close to 10 km s^{-1} for rotational velocities in the range $360-390 \text{ km s}^{-1}$. Based on the W' and W''' criteria, we confirm the O9.5 V classification.

3.3.3 *BD-13°4930 (W367)*

So far classified as O9.5 V (Hillenbrand et al. 1993), Bosch et al. (1999) noticed that the star had a peculiar velocity compared to the cluster systemic velocity, thus questioning the membership of *BD-13°4930* to NGC 6611.

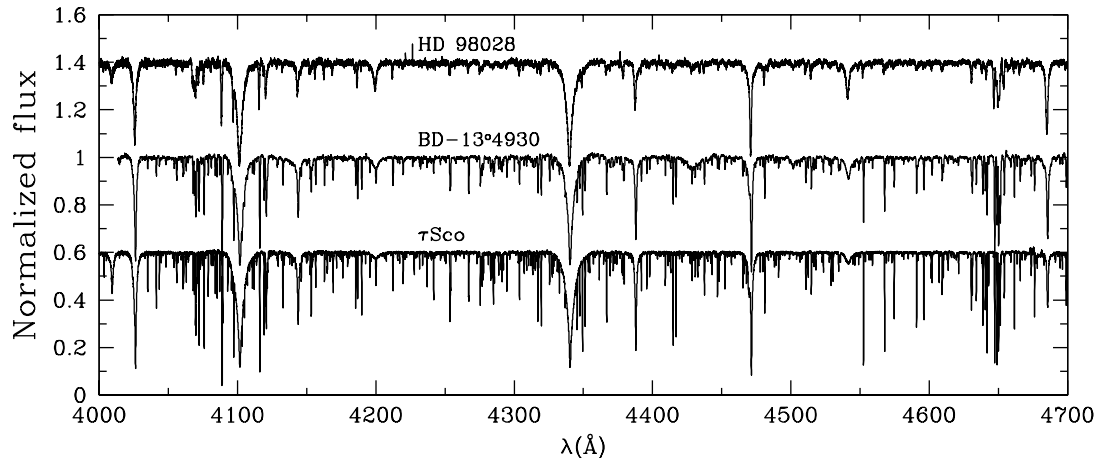


Figure 15. BD-13°4930 spectrum in the range 4000-4700 Å compared to the spectra of HD 98028 (O9 V) and τ Sco (B0.2 V).

We acquired six FEROS spectra, complemented by two GIRAFFE spectra and one FEROS spectrum from Evans et al. (2005). With an internal RV dispersion of about 1 km s^{-1} only, we could not detect any variability in our data. BD-13°4930 is definitely a slow rotator. Most of the lines display a steep Lorentzian profile although some lines, such as He I $\lambda 5876$ definitely show a Gaussian profile. The He II lines further display a broader profile than the He I lines. Using rotationally-broadened profiles for comparison, we estimated that the core of the He I lines is not compatible with a projected rotational velocity larger than 40 km s^{-1} . This is in line with earliest measurements by Dufton et al. (2006) and Hunter et al. (2007) (see Table 5). The He II $\lambda 4686$ line core indicates $v \sin i \approx 50 \text{ km s}^{-1}$; the He II $\lambda 5412$ line core, $v \sin i \approx 60 \text{ km s}^{-1}$ while the He II $\lambda 4542$ core yields $v \sin i \gtrsim 100 \text{ km s}^{-1}$. While we use a purely rotational profile for comparison, we note that the broadening of the He II lines might rather be due to the Stark broadening.

While clearly displaying the He II $\lambda\lambda 4542, 4686$ and 5412 lines typical of an O-type star (Fig. 14), BD-13°4930 also displays a large number of metallic sharp lines typical of late-O/early-B stars (Fig. 15). Considering only the He I and He II lines, our spectral classification criteria suggest an O8.5 V spectral type, with the O9 V sub-type well within $1\text{-}\sigma$. FEROS spectra of two spectral standards from Walborn & Fitzpatrick (1990), HD 93028 (O9 V) and τ Sco (B0.2 V), are available in the FEROS archive from ESO. We retrieved both of them and reduced them as described in Sect. 2. Fig. 15 provides a direct comparison of the three spectra. Clearly, BD-13°4930 displays properties at mid-course between HD 93028 and τ Sco. We thus adopt O9.5 V as our final classification.

4 OBSERVATIONAL BIASES

RV techniques alone have proved to be an efficient method to detect high-mass spectroscopic binaries. Yet, the parameter space to probe is very large. It covers 3 to 4 orders of magnitude in period, two orders of magnitude in mass (both for the primary and secondary) and the full range of eccentricities from circular orbits to eccentricities of 0.9 or above.

Table 8. Binary detection probability for the time sampling associated with different objects (Col. 1) and for various period ranges (Cols. 2 to 5).

Time sampling	Short [2-10d]	Intermed. [10-365d]	Long [365-3000d]	All [2-3000d]
BD-13°4923	0.997	0.924	0.697	0.933
BD-13°4927	0.994	0.897	0.695	0.925
BD-13°4928	0.990	0.829	0.534	0.883
BD-13°4929	0.995	0.819	0.521	0.878
BD-13°4930	0.993	0.911	0.690	0.928
HD 168075	0.995	0.913	0.667	0.848
HD 168076	0.995	0.925	0.690	0.932
HD 168137	0.995	0.942	0.727	0.943
HD 168183	0.991	0.876	0.508	0.891

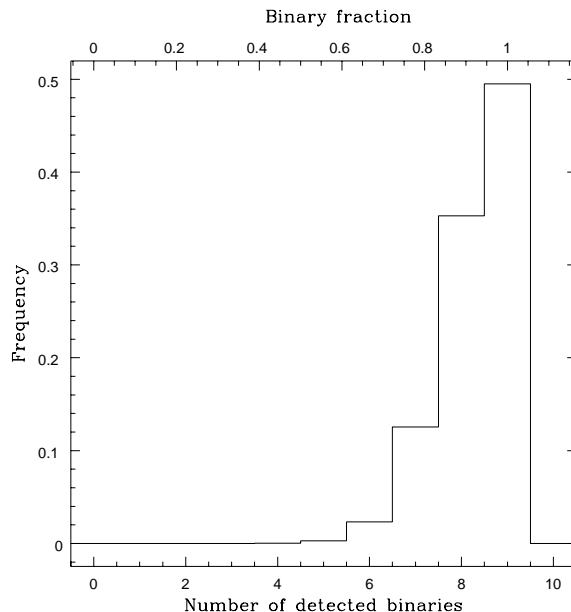


Figure 16. Distribution of the number of detected SB systems as obtained from 10 000 realisations of a cluster with nine O-type binaries.

Naturally, RV techniques are not equally sensitive in all the regions of the parameter space. This not only results from the amplitude of the RV signal but also from the very different time sampling needed to uncover a short-period system with a high mass-ratio versus a long period, eccentric object with a lower mass secondary component. As a consequence, depending on the probed location in the parameter space, a given time sampling does not allow us to unveil multiple systems with the same probability.

To better estimate the observational biases of our campaign, we have run a series of Monte-Carlo simulations using two different approaches. In the following simulations, we adopted a ΔRV threshold for the primary star of 20 km s^{-1} to consider a binary as detected.

Estimating the detection biases is unfortunately an ill-posed problem as the probability of detection in a given part of the parameter space and for a given observational sampling, needs to be convolved with the distribution of the orbital parameters which, for massive stars, are still poorly constrained. Still, reasonable estimates of the detection biases can be obtained using assumptions that are based on the results of Paper I. The period distribution is chosen to be bi-uniform in log scale, between $\log P = 0.3$ and 1.0 (days), and between 1.0 and 3.5 (days), with 60% of the systems in the former interval. The eccentricity distribution is taken to be uniform between 0.0 and 0.9 , with the additional constraint that the separation at periastron passage should be larger than $20 R_{\odot}$ in order to avoid contact. The mass-ratio distribution is chosen to be uniform between 0.2 and 1.0 .

Adopting the actual observing sampling corresponding to each object, we randomly drew 10 000 orbital configurations, adopting a random orientation of the orbital plane in space and a random time of periastron passage. Table 8 reports the detection probabilities (P_{detect}) for short, intermediate and long period binaries, as well as for the full period ranges. It indicates that our campaign is very sensitive in the short-period regime ($P_{\text{detect}} > 0.99$) while its performances remain very good up to one year ($P_{\text{detect}} \approx 0.8 - 0.9$). Beyond that, the detection probability tends to drop to $0.5 - 0.6$ typically. Yet, given that only 15% of the spectroscopic binary population is expected to have periods between one and ten years, our lower sensitivity in this range has a limited impact on the total detection probability as shown by the last column of Table 8.

As a second step, to check the consistency of the estimated individual observational biases in the context of a sample of several stars, we randomly drew nine orbital configurations for nine O stars whose masses match the observed primary masses in NGC 6611. We then applied the existing time sampling of our O-type star observations, randomly associating each time series to an object of the simulated cluster, then deducing an observed binary fraction. Repeating this for 10 000 simulated clusters, Fig. 16 shows the distribution of the detected binary fraction. It predicts that our campaign should have been able to achieve a detection rate of $0.93_{-0.10}^{+0.07}$ [0.85 confidence interval], leaving little room for undetected spectroscopic binaries.

To conclude this section, we note that our simulations do not take into account line blending, so that our adopted detection threshold might be too optimistic for SB2 binaries with similar mass and flux. Yet, a semi-amplitude of the RV-curve of several 10 km s^{-1} would already result in significant

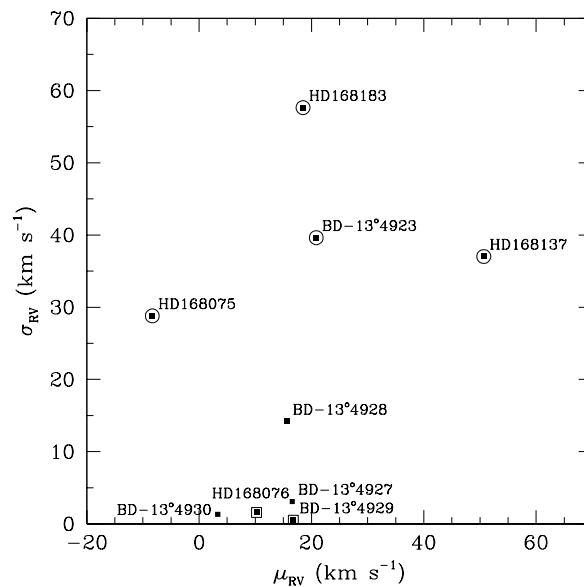


Figure 17. Dispersion of the He I $\lambda 5876$ RV measurements versus their mean RV. Circles around the $\sigma - \mu$ point indicate the gravitationally bound binaries while squares show the objects with a composite spectrum. The average systemic velocities have been used instead of the mean RV for the two binaries with orbital solutions : BD-13°4923 and HD 168183.

changes ($> 20\%$) of the line depths, so that the binary nature of those objects would be unveiled by their line profiles rather than by their RV variations. Only some of the long-period systems ($q > 0.8$, $P > 1000$ d) would likely remain undetected. This additional shading of the parameter space decreases the total detection probabilities given in Table 8 and Fig. 16 by a couple of percent, which does not qualitatively affect our conclusions.

5 DISCUSSION

5.1 Membership

Fig. 17 displays the observed $1-\sigma$ RV dispersions of the He I $\lambda 5876$ line in our sample, plotted versus the average RV measurements of the same line. In such a diagram, the vertical axis gives us an indication of the variability while the horizontal axis provides us with some indication of the cluster systemic velocity. Beyond the four gravitationally bound binaries, it is BD-13°4928 that shows the largest apparent variability. Yet, as previously discussed, the star is undergoing rapid rotation, thus broadening the spectral lines and making the exact determination of the line centroid less accurate. The remaining stars present an rms dispersion of their RV measurements of a few km s^{-1} at most and, indeed, all of them are considered to be isolated or very long period objects.

Both BD-13°4930 and HD 168076 show smaller peculiar velocities compared to the average cluster velocity ($\approx 17 \text{ km s}^{-1}$). Yet we note that HD 168076 is a possible long period binary, so that the observed shifts might be additional hints of an ongoing physical process rather than indi-

Table 9. Final spectroscopic classification and multiplicity properties of the studied O stars in NGC 6611. ‘SB2O’ means that an orbital solution has been obtained; ‘SB2E’, that the system displays eclipses in addition to its SB2 signature.

Object	Mult.	Evans et al.	Sp. Type	$q = M_2/M_1$	P (d)	e
			This work			
Gravitationally-bound systems						
BD -13° 4923	SB2O	O5 V((f+))+O	O4 V((f+))+O7.5 V	0.6	13.3	0.3
HD 168075 ^a	SB2O	O6-7 V((f))	O6.5 V((f))+B0-1 V	0.487	43.6	0.17
HD 168137	SB2	O8.5 V	O7 V+O8 V	0.75-0.8	>>30	undef.
HD 168183	SB2OE	B0 III	O9.5 III+B3-5 V/III	0.3	4.015	0.05
Composite systems						
BD -13° 4929	SB3	O9 V	O7 V+(B0.5 V+B0.5 V)	1.0+(1.0)	undef.+(~4)	undef.
HD 168076	composite	O4III ((f+))	O3.5 V((f+))+O7.5 V	0.43	>1.5 10 ⁵ ?	undef.
Single stars						
BD -13° 4927	sgl.	O7 II(f)	O7 II(f)	<i>n/a</i>	<i>n/a</i>	<i>n/a</i>
BD -13° 4928	sgl.	O9.5 Vn	O9.5 V	<i>n/a</i>	<i>n/a</i>	<i>n/a</i>
BD -13° 4930	sgl.	O9.7 IIIp	O9.5 Vp	<i>n/a</i>	<i>n/a</i>	<i>n/a</i>

a. Orbital parameters for HD 168075 are taken from Barbá et al. (2009).

cations of non-membership. Assuming BD -13° 4930 is not a member of NGC 6611, the following discussion would mostly remain unaffected.

5.2 Binary fraction

With four definite SB2 gravitationally bound systems out of nine objects in our sample, the minimal binary fraction is $f_{\min} \sim 0.44$. As discussed in Sect. 3.2, two objects display an apparently composite spectrum and could be long period binaries if physically bound. Summing up those binary candidates would increase the binary fraction f up to 0.67. From Table 8, one can further conclude that there is little room for non-detection biases for the remaining three stars, making them likely single. For the sake of the present discussion, we will adopt a formal binary fraction of $f = 0.55 \pm 0.11$ in our sample.

Using the same reasoning as in Paper I, and assuming that the O stars in our sample are randomly drawn from a binomial parent distribution, we infer a minimal binary fraction for the parent distribution of 0.33 at the 0.01 **significance** level. We note that both the binary fraction and the constraints on the parent distribution parameters are compatible with the results obtained for NGC 6231 (see Paper I). Yet the detailed estimate of the detection biases done in Sect. 4 allows us to address another aspect of the parent distribution. Fig. 16 reveals that the likelihood to detect five or fewer binaries under the hypothesis that all the O stars in NGC 6611 are binaries amounts to 0.003 only. As a consequence, our observations are not compatible with a contemporaneous multiplicity rate of 100%.

5.3 Orbital parameters

While our campaign cannot allow us to derive the complete set of orbital parameters of all the SB2 systems, the periods and mass-ratios are reasonably well constrained (Table 9). The binary fraction in NGC 6611 is similar to the

Table 10. New spectroscopic distance moduli (DM) for the O stars in this work.

Object	$E(B - V)$	V_0	$M_V^{\text{th.}}$	DM
BD -13° 4923	1.26±0.02	5.29±0.15	-5.85	11.14±0.15
HD 168076	0.71±0.10	5.52±0.38	-5.94	11.46±0.38
HD 168075	0.81±0.11	5.74±0.41	-5.65	11.39±0.41
HD 168183	0.60±0.10	5.94±0.38	-5.20	11.14±0.38
BD -13° 4929	0.98±0.21	6.17±0.81	-5.24	11.41±0.81
HD 168137	0.68±0.03	6.42±0.12	-5.33	11.75±0.12
BD -13° 4927	0.94±0.61	7.59±2.34	-5.54	13.13±2.34
BD -13° 4928	0.76±0.05	7.19±0.20	-3.90	11.09±0.20
BD -13° 4930	0.60±0.08	7.11±0.31	-4.34	11.45±0.31

one in NGC 6231 (Paper I). Yet, NGC 6611 lacks the over-abundant short-period population seen in NGC 6231. This however might result from the small size of our sample. A Kolmogorov-Smirnov test does indeed not authorize to reject the hypothesis that the two samples are taken from the same underlying distribution. Similarly, the distributions of mass ratios in the two clusters are in good agreement and are both compatible with a uniform distribution from $q = 1$ to $q = 0.2 - 0.3$ (the observational limit for secondary detection in massive spectroscopic binaries). Finally, we note that the location, in the period-eccentricity diagram, of the systems with known eccentricity would remain well within the area normally populated by O-type binaries.

5.4 Companion mass function

With two O+O and two O+B binaries, plus two additional O+OB candidates, the secondary companion of an O-type star in NGC 6611 is strongly biased towards higher masses. Indeed, only three systems, the presumably single stars, could still hide undetected, low-mass companions. As we pointed out in Paper I, the mass of an O star companion cannot be randomly drawn from a normal initial mass function.

5.5 Distance

Using the new spectral classification listed in Table 9, we estimated the spectroscopic distance moduli of each star. This ultimate check allows not only to test the agreement between the spectral types and the object brightnesses, but allows for an independent estimate of the cluster distance. For this purpose, we adopted the calibration of Martins & Plez (2006) for O stars and the one of Humphreys & McElroy (1984) for B stars. For multiple objects, we weighted the intrinsic color excess $E(B - V)$ and the bolometric correction by the expected contributions of the components to the total flux. Errors were estimated by means of the error propagation, adopting a dispersion corresponding to half a sub-spectral type on the parameters taken from the calibrations. The reddening law is taken to be $A_V = 3.75E(B - V)$ (Hillenbrand et al. 1993). Table 10 lists the visual magnitude corrected for reddening (V_0), the expected absolute magnitude given the component spectral types (M_V^{th}) and the corresponding distance moduli (DM). Given the estimated error-bars, the latter are in very good agreement with each other. A weighted average gives $\overline{DM} = 11.4 \pm 0.1$. This corresponds to a distance to NGC 6611 of $d = 1.9 \pm 0.1$ kpc, in excellent agreement with the estimate of Dufton et al. (2006).

6 SUMMARY

Using a set of about 100 medium- to high-resolution spectra collected over several years, we revisited the properties of the current O-type star population of NGC 6611 in the Eagle Nebula, with a particular emphasis on their spectral classification and multiplicity.

We unveiled several new binaries and confirmed two suspected candidates. We proposed the first SB2 solutions for BD-13°4923 and HD 168183. We further identified several objects, possible long-period systems, displaying a composite spectrum. We detected the secondary companion signature for all the detected binaries allowing us to put important constraints on the mass-ratio distribution and on the distribution of secondary masses. As a support to our analysis, we further present a set of Monte-Carlo simulations that assess the binary detection biases of our campaign and show that the latter do not affect our conclusions.

The minimal binary fraction is $f_{\text{min}} \approx 0.44$ but can be as large as 0.67 if the two composite objects are confirmed to be gravitationally bound. In all cases, our current data set excludes a 100% binary fraction in NGC 6611. Still, up to 75% of the total O-type star population is to be found in multiple systems. The period and mass-ratio distributions obtained are both compatible with those derived in Paper I for NGC 6231, although the two samples suffer from low-number statistics. All the detected companions are O or early- to mid-B stars, suggesting again that the secondary companion of an O-type star cannot be randomly drawn from a classical mass function but has a mass strongly biased towards the upper range of the mass spectrum.

Finally, we could not detect any significant difference in the multiplicity properties of the O star population of NGC 6611 and NGC 6231. The environmental properties in which those two populations evolved are however significantly different. On the one hand, NGC 6611 is likely very

young, about 1 to 2 Myr old as attested by the presence of two O3-4 stars but no Wolf-Rayet object, and still very dusty. On the other hand, NGC 6231 is significantly older (around 3-4 Myr) and has already cleared out its dust.

The results presented here and the significant revision of the status of several objects despite the relative proximity of the cluster and the abundant literature on its O-star population shows the need to pursue our effort on several other nearby clusters. Only upon completion of our campaign will we be able to draw a global picture of the properties of the O-type star population in the nearby Universe.

ACKNOWLEDGMENTS

The authors are grateful to R. Barbá for sharing results before publication and to the referee, D. Gies, for a careful revision of the manuscript. This paper relies on data taken at the La Silla-Paranal Observatory under program IDs 71.C-0513, 171.D-0237, 073.D-0234, 073.D-0609, 075.D-0061, 075.D-0369, 077.D-0146, 079.D-0564 and 082.D-0136(A). This paper also made use of the ADS, of the SIMBAD and WEBDA databases and of the Vizier catalogue access tool (CDS, Strasbourg, France).

REFERENCES

- Barbá R., et al. 2009, in The interferometric view of hot stars, Rev. Mex. Conf. Ser., Eds. T. Rivinius et al., in press
- Bevington P., 1969, Data Reduction and Error Analysis for the Physical Sciences, McGraw-Hill Book Company, Inc., USA
- Bonatto C., Santos Jr. J. F. C., Bica E., 2006, A&A, 445, 567
- Bosch G. L., Morrell N. I., Niemelä V. S., 1999, Revista Mexicana de Astronomia y Astrofisica, 35, 85
- Conti P. S., 1973, ApJ, 179, 181
- Conti P. S., Alschuler W. R., 1971, ApJ, 170, 325
- Conti P. S., Leep E. M., Lorre J. J., 1977, ApJ, 214, 759
- Duchêne G., Simon T., Eisloffel J., Bouvier J., 2001, A&A, 379, 147
- Dufton P. L., Smartt S. J., Lee J. K., Ryans R. S. I., Hunter I., Evans C. J., Herrero A., Trundle C., Lennon D. J., Irwin M. J., Kaufer A., 2006, A&A, 457, 265
- Evans C. J., Smartt S. J., Lee J.-K., Lennon D. J., Kaufer A., Dufton P. L., Trundle C., Herrero A., et al. 2005, A&A, 437, 467
- Gosset E., Royer P., Rauw G., Manfroid J., Vreux J.-M., 2001, MNRAS, 327, 435
- Guarcello M. G., Prisinzano L., Micela G., Damiani F., Peres G., Sciortino S., 2007, A&A, 462, 245
- Gvaramadze V. V., Bomans D. J., 2008, A&A, 490, 1071
- Heck A., Manfroid J., Mersch G., 1985, A&AS, 59, 63
- Hester J. J., Scowen P. A., Sankrit R., Lauer T. R., Ajhar E. A., Baum W. A., Code A., Currie D. G., et al. 1996, AJ, 111, 2349
- Hillenbrand L. A., Massey P., Strom S. E., Merrill K. M., 1993, AJ, 106, 1906
- Hipparcos Catalogue 1997, in Perryman M. A. C., ESA Special Publication Vol. 1200

- Hobbs L. M., York D. G., Snow T. P., Oka T., Thorburn J. A., Bishof M., Friedman S. D., McCall B. J., Rachford B., Sonnentrucker P., Welty D. E., 2008, *ApJ*, 680, 1256
- Humphreys R. M., McElroy D. B., 1984, *ApJ*, 284, 565
- Hunter I., Dufton P. L., Smartt S. J., Ryans R. S. I., Evans C. J., Lennon D. J., Trundle C., Hubeny I., Lanz T., 2007, *A&A*, 466, 277
- Martayan C., Floquet M., Hubert A. M., Neiner C., Frémat Y., Baade D., Fabregat J., 2008, *A&A*, 489, 459
- Martins F., Plez B., 2006, *A&A*, 457, 637
- Martins F., Schaerer D., Hillier D., 2005, *A&A*, 436, 1049
- Mathys G., 1988, *A&AS*, 76, 427
- Mathys G., 1989, *A&AS*, 81, 237
- Oliveira J. M., 2008, *Handbook of Star Forming Regions*. in press
- Sana H., 2009, *A&A*, 501, 291
- Sana H., Gosset E., 2009, *A&A*, submitted
- Sana H., Gosset E., Nazé Y., Rauw G., Linder N., 2008, *MNRAS*, 386, 447
- Underhill A. B., 1994, *ApJ*, 420, 869
- Walborn N. R., Fitzpatrick E. L., 1990, *PASP*, 102, 379
- Walborn N. R., Howarth I. D., Lennon D. J., Massey P., Oey M. S., Moffat A. F. J., Skalkowski G., Morrell N. I., Drissen L., Parker J. W., 2002, *AJ*, 123, 2754
- Walker M. F., 1961, *ApJ*, 133, 438
- Wolff S. C., Strom S. E., Dror D., Venn K., 2007, *AJ*, 133, 1092

This paper has been typeset from a $\text{T}_{\text{E}}\text{X}/\text{L}^{\text{A}}\text{T}_{\text{E}}\text{X}$ file prepared by the author.